

Nanoscale Assemblies of Gigantic Molecular $\{\text{Mo}_{154}\}$ -Rings: (Dimethyldioctadecylammonium) $_{20}[\text{Mo}_{154}\text{O}_{462}\text{H}_8(\text{H}_2\text{O})_{70}]$

Tomoyuki Akutagawa,^{*,†,‡,§} Reina Jin,[‡] Ryo Tunashima,[†] Shin-ichiro Noro,^{†,‡}
Leroy Cronin,^{*,||} and Takayoshi Nakamura^{*,†,‡,§}

Research Institute for Electronic Science, Hokkaido University, Sapporo 060-0812, Japan, Graduate School of Environmental Earth Science, Hokkaido University, Sapporo 060-0810, Japan, CREST, Japan Science and Technology Agency (JST), Kawaguchi 332-0012, Japan, and WestCHEM, Department of Chemistry, University of Glasgow, Glasgow G12 8QQ, UK

Received May 11, 2007. In Final Form: August 20, 2007

Clusters based on the mixed-valence gigantic inorganic ring $[\text{Mo}_{154}\text{O}_{462}\text{H}_{14}(\text{H}_2\text{O})_{70}]^{14-}$ ($\{\text{Mo}_{154}\}$ -ring) and dimethyldioctadecylammonium (DODA) were combined to form novel molecular assemblies of an inorganic–organic hybrid molecular system as Langmuir–Blodgett (LB) and cast films. $(\text{DODA})_{20}[\text{Mo}_{154}\text{O}_{462}\text{H}_8(\text{H}_2\text{O})_{70}]$ (**2**) was prepared by cation exchange and was characterized by a combination of thermogravimetry, IR, UV–vis–NIR, ¹H NMR, and XRD measurements. The salt **2** was soluble in common organic solvents, and the chemical stability of $\{\text{Mo}_{154}\}$ -ring encapsulated by DODA cationic surfactants in CHCl_3 was found to be higher than that of the “native” sodium salt of the $\{\text{Mo}_{154}\}$ -ring in H_2O . Uniform spherical vesicle-like molecular assemblies of $(\text{DODA})_{20}[\text{Mo}_{154}\text{O}_{462}\text{H}_8(\text{H}_2\text{O})_{70}]$ were observed in dilute THF, whose average diameter of 95 nm and a normalized variance of 5.7% were confirmed by a X-ray small-angle scattering. Deposition of **2** as a cast film showed circular domains with a typical diameter of ~ 100 nm, indicating possible similarities between solution and surface-deposited structures. The resulting LB films of salt **2** were transferred from an acidic buffer subphase with $\text{pH} = 1.5$ onto mica, giving a two-dimensional film surface with a unity transfer ratio. Further, the electronic absorption spectra of the LB multilayer were consistent with the classic type II mixed-valence $\text{Mo}^{\text{V}}/\text{Mo}^{\text{VI}}$ electronic state well known for molybdenum blue $\{\text{Mo}_{154}\}$ -ring systems, and it appears that on the surface the plane of the $\{\text{Mo}_{154}\}$ -ring is approximately parallel to the substrate surface, as indicated by polarized electronic spectra, while the alkyl chains of DODA were relatively normal to the substrate surface. Therefore, the layer between the $\{\text{Mo}_{154}\}$ -rings and DODA cations was alternately stacked along the direction of film propagation. Finally, it was found that the surface morphology of the cast and LB films was determined by the molecular assembly of $(\text{DODA})_{20}[\text{Mo}_{154}\text{O}_{462}\text{H}_8(\text{H}_2\text{O})_{70}]$ in solution and the air–water interface, respectively.

Introduction

Electrically active nanomaterials such as carbon nanotubes, semiconductor nanowires, metal nanoparticles, and their complex structures on solid substrates fabricated by self-assembly processes have been extensively examined due to the possibility of discovering new physical properties and the great promise of future device applications.¹ Although the size and structure of relatively small molecules can be controlled exactly by chemical synthesis, many types of nanomaterials usually can be represented as an ensemble of entities with significant distributions in size and shape,^{1,2} which affect largely the physical properties and device performances. For example, the size distribution of gold nanoparticles prepared by citric acid reduction technique can be extended over 10%.³ Therefore, structurally well-defined na-

nomaterials represent a significant challenge, especially when precisely designed building blocks are required to construct electrically active nanostructures.

Several examples of the size-controllable nanomaterials have been known, which range from oligomers and dendrimers to inorganic clusters such as zeolites and polyoxometalates (POMs).^{1–4} In 1995, the synthesis and crystal structure of a gigantic ring-shaped POM cluster of the type $[\text{Mo}_{154}\text{O}_{462}\text{H}_{14}(\text{H}_2\text{O})_{70}]^{14-}$ ($\{\text{Mo}_{154}\}$ -ring) was first reported by Müller et al.,^{5a} and later this was followed by a much more facile synthesis of the analogous compound, $\text{Na}_{14}[\text{Mo}_{154}\text{O}_{462}\text{H}_{14}(\text{H}_2\text{O})_{70}] \cdot 400\text{H}_2\text{O}$ (**1**).^{5b,c} Since the discovery of the $\{\text{Mo}_{154}\}$ “big-wheel”, a large number of gigantic POMs, such as the $\{\text{Fe}_{30}\text{Mo}_{72}\}$ -ball,^{6d} $\{\text{Mo}_{132}\}$ -ball,^{6c,e,g,i} $\{\text{Mo}_{176}\}$ -ring,^{6a,b} $\{\text{Mo}_{248}\}$ -wheel,^{6h} and $\{\text{Mo}_{368}\}$ -lemon,^{6j} have been structurally identified.⁶ These

* Corresponding authors. T.A. and T.N.: phone, +81-11-706-2884; fax, +81-11-706-4972; e-mail, takuta@es.hokudai.ac.jp (T.A.) and tnaka@es.hokudai.ac.jp (T.N.). L.C.: phone, 0141 330 6650; fax, 0141 330 4888; e-mail, L.Cronin@chem.gla.ac.uk.

† Research Institute for Electronic Science, Hokkaido University.

‡ Graduate School of Environmental Science, Hokkaido University.

§ CREST, JST.

|| University of Glasgow.

(1) (a) *The Chemistry of Nanostructured Materials*; Young, P., Ed.; World Scientific: River Edge, NJ, 2005. (b) Guozhong, C. *Nanostructures and Nanomaterials*; Imperial College Press: Singapore, 2004. (c) *Nanoparticles*; Schmid, G., Ed.; VCH: Weinheim, 2004. (d) *Chemistry of Nano-molecular Systems—Toward the Realization of Molecular Devices*; Sugiura, K., Matsumoto, T., Tada, H., Nakamura, T., Eds.; Springer-Verlag: Berlin, 2002.

(2) *Nanoscale Materials in Chemistry*; Klabunde, K. L., Ed.; Wiley & Sons: New York, 2001.

(3) (a) Daniel, M.-C.; Astruc, D. *Chem. Rev.* **2004**, *104*, 293. (b) Grabar, K. C.; Freeman, R. G.; Hommer, M. B.; Naten, M. J. *Anal. Chem.* **1995**, *67*, 735.

(4) (a) Müller, A.; Kögerler, P.; Kuhlmann, C. *Chem. Commun.* **1997**, 1437. (b) Müller, A.; Kögerler, P.; Dress, A. W. M. *Coord. Chem. Rev.* **2001**, *222*, 193. (c) Müller, A.; Serani, C. *Acc. Chem. Res.* **2000**, *32*, 2. (d) Müller, A.; Roy, S. *Coord. Chem. Rev.* **2003**, *245*, 153. (e) *Polyoxometalate Molecular Science*; Borrás-Almenar, J. J.; Coronado, E.; Müller, A.; Pope, M., Eds.; Kluwer Academic Publishers: London, 2001. (f) *Polyoxometalate Chemistry From Topology via Self-Assembly to Applications*; Pope, T., Müller, A., Eds.; Kluwer Academic Publishers: London, 2001. (g) *Polyoxometalate Chemistry for Nano-Composite Design*; Yamase, T., Pope, M. T., Eds.; Kluwer Academic Publishers: New York, 2002. (h) Cronin, L. In *Comprehensive Coordination Chemistry II*, Amsterdam, Elsevier, Vol. 7, pp 1–57. (i) Long, D.-L.; Burkholder, E.; Cronin, L. *Chem. Soc. Rev.* **2007**, *36*, 105.

(5) (a) Müller, A.; Krickemeyer, E.; Meyer, J.; Bögge, H.; Peters, F.; Plass, W.; Diemann, E.; Dillinger, S.; Nonnenbruch, F.; Randerath, M.; Menke, C. *Angew. Chem., Int. Ed. Engl.* **1995**, *34*, 2122. (b) Müller, A.; Das, S. K.; Krickemeyer, E.; Kuhlmann, C. In *Inorganic Syntheses*; Shapley, J. R., Ed.; Wiley: New York, 2004; p 191. (c) Müller, A.; Das, S. K.; Fedin, V. P.; Krickemeyer, E.; Beugholt, C.; Bögge, H.; Schmidtman, M.; Hauptfleisch, B. *Z. Anorg. Chem.* **1999**, *625*, 1187.

structurally well-defined POM clusters represent some of the most important candidates for the controlled and reproducible size-controllable electrically active nanomaterials.⁴ Furthermore, the rich redox properties of associated with POMs means that they are very suitable as precursors for the construction of electrically and magnetically active materials.⁷ For example, the electron-accepting ability of [PMo₁₂O₄₀] in CH₃-CN is comparable to that of the typical electron acceptor 7,7,8,8-tetracyano-*p*-quinodimethane (TCNQ).⁸ Notably the reduction of α -[PMo₁₂O₄₀]³⁻ allows the formation of a stable one-electron-reduced α -[PMo₁₂O₄₀]⁴⁻ and two-electron-reduced α -[PMo₁₂O₄₀]⁵⁻ in solution and the solid state.⁹ Indeed, partially reduced POM clusters,¹⁰ especially gigantic POMs such as {Mo₁₃₂}-ball and {Mo₁₅₄}-ring, have potential to be used in the formation of electrically and magnetically active materials.^{4,7}

Although a large number of crystal structures of gigantic POMs have been reported so far,⁴⁻⁶ the assembly of gigantic POMs on the substrate surface has not been extensively studied. However, Clemente-León and Coronado first reported Langmuir-Blodgett (LB) films of Keggin-type [XW₁₂O₄₀] (X = P, As, Si, B, and Co) polyanions in 1997.¹¹ Since this work, around 20 POM-based LB films have been reported.^{11,12} However, almost all of these were constructed from relatively low nuclearity and fully

oxidized POMs. Recently, several LB films of gigantic POMs such as {Mo₁₃₂}-ball, {Mo₅₇V₆}, {Mo₅₇Fe₆}, and {Mo₁₄₂}-ring have been reported utilizing the dimethyldioctadecylammonium cation (DODA) as a counter cation,^{13,14} which introduces amphiphilic-like properties to the POM-cation hybrid, rendering these systems as excellent candidates for the formation of LB-films. In the fabrication of LB films of {Mo₁₄₂}-ring,¹⁴ (DODA)(Br) was spread on the aqueous subphase containing [Mo₁₄₂O₄₂₉H₁₀(H₂O)₄₉(CH₃CO₂)₅(CH₃CH₂CO₂)₂₈]²⁸⁻, and the floating monolayer was transferred onto the substrate surfaces. Within the LB films, the lamellar-type layer structure between the {Mo₁₄₂}-rings and DODA cations was confirmed by X-ray reflectivity measurements, in which the {Mo₁₄₂}-ring plane was relatively parallel to the substrate surface and DODA cations lie on the {Mo₁₄₂}-ring plane.

We have been highly interested in investigating and exploiting the tendency of the gigantic {Mo₁₅₄}-ring to aggregate and form vesicle-like "blackberry" assemblies in solution, which resemble vesicle/micelle-like architectures.¹⁵ Since micelles and vesicles are typically found from organic surfactants,¹⁶ in which the intermolecular interaction between polar head and hydrophobic tail of the surfactant molecule is essential to reduce the free energy of the spherical molecular assembly, we considered that the formation of hybrid-ring organocation conjugates may lead to systems that can self-assemble in solution. Although the {Mo₁₅₄}-ring does not present hydrophobic properties, the formation of a vesicle-like molecular assembly of Na₁₄-[Mo₁₅₄O₄₆₂H₁₄(H₂O)₇₀] was confirmed by dynamic light scattering measurements in H₂O,¹⁵ and the high intrinsic tendency of the {Mo₁₅₄}-ring to aggregate in solution is clear and it could be expected to form novel nanoscale molecular assemblies on the substrate surface. From this point of view, we examined the LB and cast films of a {Mo₁₅₄}-ring encapsulated by DODA cationic surfactants on substrates. The cation exchange reaction of salt **1** from sodium to DODA yielded solid (DODA)₂₀[Mo₁₅₄O₄₆₂H₈(H₂O)₇₀] (**2**), and the nanoscale dimensions of the molecular structure of {Mo₁₅₄}-ring are illustrated in Scheme 1. The diameters of the inorganic ring and inner void space are about 3.7 and 2.0 nm, respectively, while the height of ring is about 1.5 nm and the cross-sectional area of the {Mo₁₅₄}-ring plane is ~10.8 nm². The length of two octadecyl chains with the all-

(6) (a) Müller, A.; Krickemeyer, E.; Bögge, H.; Schmidtman, M.; Beugholt, C.; Kögerler, P.; Lu, C. *Angew. Chem., Int. Ed.* **1998**, *37*, 1220. (b) Müller, A.; Koop, M.; Bögge, H.; Schmidtman, M.; Beugholt, C. *Chem. Commun.* **1998**, 1501. (c) Müller, A.; Shah, S. Q. N.; Bögge, H.; Schmidtman, M.; Kögerler, P.; Hauptfleisch, B.; Leiding, S.; Wittler, K. *Angew. Chem., Int. Ed.* **2000**, *39*, 1614. (d) Müller, A.; Sarkar, S.; Shah, S. Q. Z.; Bögge, H.; Schmidtman, M.; Sarkar, S.; Kögerler, P.; Hauptfleisch, B.; Trautwein, A. X.; Schünemann, V. *Z. Angew. Chem., Int. Ed.* **1999**, *38*, 3238. (e) Müller, A.; Fedin, V. P.; Kuhlmann, C.; Bögge, H.; Schmidtman, M. *Chem. Commun.* **1999**, 927. (f) Yamase, T.; Prokop, P.; Arai, Y. *J. Mol. Struct.* **2003**, *656*, 107. (g) Müller, A.; Das, S. K.; Kögerler, P.; Bögge, H.; Schmidtman, M.; Roy, S.; Berkle, A. *Angew. Chem., Int. Ed.* **2002**, *41*, 3604. (j) Müller, A.; Beckmann, E.; Bögge, H.; Schmidtman, M.; Dress, A. *Angew. Chem., Int. Ed.* **2002**, *41*, 1162.

(7) (a) Gatteschi, D.; Pardi, L.; Barra, A. L.; Müller, A.; Döring, J. *Nature* **1991**, *354*, 463. (b) Ouahab, L.; Grandjean, D.; Bencharif, M. *Acta Crystallogr. Sect. C* **1991**, *47*, 2670. (c) Ouahab, L.; Bencharif, M.; Mhanni, A.; Pelloquin, D.; Halet, J.-F.; Peña, O.; Padiou, J.; Grandjean, D.; Garrigou-Lagrange, C.; Amiel, J.; Delhaès, P. *Chem. Mater.* **1992**, *4*, 666. (d) Maguerès, P. L.; Ouahab, L.; Golhen, S.; Grandjean, D.; Pena, O.; Jegaden, J.-C.; Gómez-García, C. J.; Delhaès, P. *Inorg. Chem.* **1994**, *33*, 5180. (e) Gómez-García, C. J.; Ouahab, L.; Giménez-Saiz, C.; Triki, S.; Coronado, E.; Delhaès, P. *Angew. Chem., Int. Ed. Engl.* **1994**, *33*, 223. (f) Galan-Mascarós, J. R.; Giménez-Saiz, C.; Triki, S.; Gómez-García, J. R.; Coronado, E.; Ouahab, L. *Angew. Chem., Int. Ed. Engl.* **1995**, *34*, 1460. (g) Bellitto, C.; Bonamico, M.; Fares, V.; Federici, F.; Righini, G.; Kurmoo, M.; Day, P. *Chem. Mater.* **1995**, *7*, 1475. (h) Coronado, E.; Galan-Mascarós, J. R.; Giménez-Saiz, C.; Gómez-García, C. J.; Triki, S. *J. Am. Chem. Soc.* **1998**, *120*, 4671. (i) Coronado, E.; Galan-Mascarós, J. R.; Giménez-Saiz, C.; Gómez-García, C. J.; Falvello, L. R.; Delhaès, P. *Inorg. Chem.* **1998**, *37*, 2183. (j) Coronado, E.; Gómez-García, C. J. *Chem. Rev.* **1998**, *98*, 273. (k) Müller, A.; Peters, F.; Pope, M. T.; Gatteschi, D. *Chem. Rev.* **1998**, *98*, 239. (l) Coronado, E.; Giménez-Saiz, C.; Gómez-García, C. J.; Capelli, S. J. *Angew. Chem., Int. Ed.* **2004**, *43*, 3022. (m) Nyman, M.; Ingersoll, D.; Singh, S.; Bonhomme, F.; Alam, T. M.; Brinker, C. J.; Rodriguez, M. A. *Chem. Mater.* **2005**, *17*, 2885. (n) Coronado, E.; Galán-Mascarós, J. R.; Giménez-Saiz, C.; Gómez-García, C. J.; Martínez-Ferrero, E.; Almeida, M.; Lopes, E. B.; Capelli, S. C.; Llusar, R. M. *J. Mater. Chem.* **2004**, *14*, 1867.

(8) (a) Sadakane, M.; Steckhan, E. *Chem. Rev.* **1998**, *98*, 219. (b) Akutagawa, T.; Endo, D.; Imai, H.; Noro, S.; Cronin, L.; Nakamura, T. *Inorg. Chem.* **2006**, *45*, 8626.

(9) (a) Varga, G. M.; Papaconstantinou, E.; Pope, M. T. *Inorg. Chem.* **1970**, *9*, 662. (b) Casa'n-Pastor, N.; Baker, C. W. *J. Am. Chem. Soc.* **1992**, *114*, 10384. (c) Neier, R.; Trojanowski, C.; Mattes, R. *J. Chem. Soc. Dalton Trans.* **1995**, 2521. (d) Mialane, P.; Dolbecq, A.; Linsard, L.; Mallard, A.; Marrot, J.; Sécheresse, F. *Angew. Chem., Int. Ed.* **2002**, *41*, 2398. (e) Wang, X.; Qin, C.; Wang, E.; Su, Z.; Li, Y.; Xu, L. *Angew. Chem., Int. Ed.* **2006**, *45*, 7411.

(10) (a) Prados, R. A.; Meiklejohn, P. T.; Pope, M. T. *J. Am. Chem. Soc.* **1974**, *96*, 1261. (b) Prados, R. A.; Pope, M. T. *Inorg. Chem.* **1976**, *15*, 2547. (c) Sanchez, C.; Livage, J.; Launary, J. P.; Fournier, M.; Jeannin, Y. *J. Am. Chem. Soc.* **1982**, *104*, 3194.

(11) (a) Clemente-León, Agricole, B.; Mingotaud, C.; Gómez-García, C. J.; Coronado, E.; Delhaès, P. *Langmuir* **1997**, *13*, 2340. (b) Clemente-León, Mingotaud, C.; Agricole, B.; Gómez-García, C. J.; Coronado, E.; Delhaès, P. *Angew. Chem., Int. Ed. Engl.* **1997**, *36*, 1114.

(12) (a) Clemente-León, M.; Coronado, E.; Soriano-Portillo, A.; Mingotaud, C.; Dominguez-Vera, J. M. *Adv. Colloid Interface Sci.* **2005**, *116*, 193. (b) Ito, T.; Sawada, K.; Yamase, T. *Chem. Lett.* **2003**, *32*. (c) Wang, J.; Wang, H. S.; Fu, L. S.; Liu, F. Y.; Zhang, H. J. *Thin Solid Films* **2002**, *414*, 256. (d) Wang, J.; Wang, H.; Fu, L.; Liu, F.; Zhang, H. *Thin Solid Films* **2002**, *415*, 242. (e) Nyman, M.; Ingersoll, D.; Singh, S.; Bohomme, F.; Alam, T. M.; Brinker, C. J.; Rodriguez, M. A. *Chem. Mater.* **2005**, *17*, 2885. (f) Liu, S.; Möhwald, H.; Volkmer, D.; Kurth, D. G. *Langmuir* **2006**, *22*, 1949. (g) Wang, L.; Wang, E.; Hao, N.; Jiang, M.; Wang, Z.; Lü, J.; Xu, L. *J. Colloid Interface Sci.* **2004**, *274*, 602. (h) Ito, H.; Yashiro, H.; Yamase, T. *Langmuir* **2006**, *22*, 2806. (i) Yang, G.; Guo, H.; Wang, M.; Huang, M.; Chen, H.; Liu, B.; Dong, S. *J. Electroanal. Chem.* **2007**, *600*, 318.

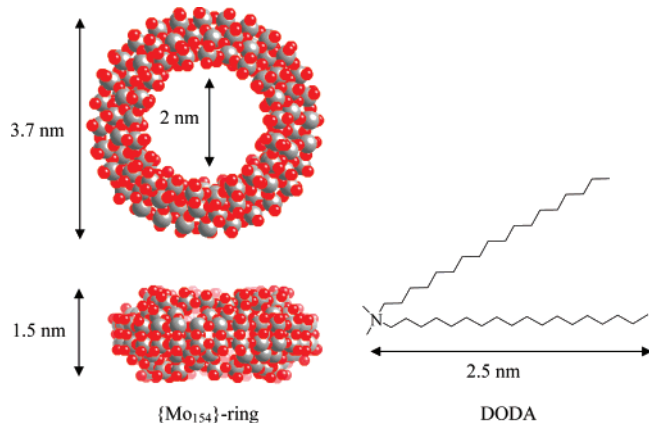
(13) (a) Kurth, D. G.; Lehmann, P.; Volkmer, D.; Müller, A.; Schwahn, D. *J. Chem. Soc. Dalton Trans.* **2000**, 3989. (b) Kurth, D. G.; Lehmann, P.; Volkmer, D.; Gölfen, H.; Koop, M. J.; Müller, A.; Chesne, A. D. *Chem. Eur. J.* **2000**, *6*, 385. (c) Volkmer, D.; Chesne, A. D.; Kurth, D. G.; Schnablegger, H.; Lehmann, P.; Koop, M. J.; Müller, A. *J. Am. Chem. Soc.* **2000**, *122*, 1995. (d) Clemente-León, M.; Coronado, E.; Gómez-García, C. J.; Mingotaud, C.; Ravaine, S.; Romualdo-Torres, G.; Delhaès, P. *Chem. Eur. J.* **2005**, *11*, 3979.

(14) (a) Clemente-León, M.; Ito, T.; Yashiro, H.; Yamase, T.; Coronado, E. *Langmuir* **2007**, *23*, 4042. (b) Clemente-León, M.; Ito, T.; Yashiro, H.; Yamase, T. *Chem. Mater.* **2007**, *19*, 2589.

(15) (a) Müller, A.; Diemann, E.; Kuhlmann, C.; Eimer, W.; Serain, C.; Tak, T.; Knöchel, A.; Pranzas, K. *Chem. Commun.* **2001**, 1928. (b) Liu, T. *J. Am. Chem. Soc.* **2002**, *124*, 10942. (c) Liu, T.; Diemann, E.; Dress, A. W. M.; Müller, A. *Nature* **2003**, *426*, 59. (d) Liu, T. *J. Am. Chem. Soc.* **2003**, *125*, 312. (e) Liu, G.; Liu, T.; Sankar, M.; Kortz, U. *J. Am. Chem. Soc.* **2006**, *128*, 10103. (f) Kistler, M. L.; Bhatt, A.; Liu, G.; Casa, D.; Liu, T. *J. Am. Chem. Soc.* **2007**, *129*, 6453.

(16) (a) Israelachvili, J. N. *Intermolecular and Surface Forces*; Academic Press: London, 1992. (b) Hamley, I. W. *Introduction of Soft Matter—Polymers, Colloids, Amphiphiles and Lipid Crystals*; Springer-Verlag: Tokyo, 2000.

Scheme 1. Molecular Structures and Dimensions of $\{Mo_{154}\}$ -Ring and DODA Cation with All-Trans Isomer



trans isomer elongated from the central positively charged nitrogen atom of DODA is about 2.5 nm, and the structurally defined nanoscale molecular assembly of the hybrid material mediated by electrostatic interactions between the $\{Mo_{154}\}$ -ring polyanion and DODA cation is expected.

Experimental Section

General. Polarized UV–vis–NIR (300–3000 nm) and IR (400–7800 cm^{-1}) spectra were measured using a Perkin-Elmer Lambda-19 spectrophotometer and a Perkin-Elmer Spectrum 2000 spectrometer, respectively. Monolayers and LB films were formed using a conventional LB trough (NIMA 632D1D2) equipped with two symmetrical moving barriers. Hydrophobic treatments of quartz and CaF_2 substrates for optical measurements were carried out using a five-layer deposition of Cd^{2+} -arachidate at a constant surface pressure (30 $mN m^{-1}$), while that of glass for XRD measurements was carried out by an immersion of glass substrates into hexamethyldisilazane (HMDS). AFM images were taken using a Seiko SPA 400 with SPI 3800 and JEOL JSPM-5200 probe stations operating at a dynamic force mode. Commercially available Si cantilevers with a force constant of 20 $N m^{-1}$ for SPA 400 and 1.5 $N m^{-1}$ for JSPM-5200 were used. SEM images of cast films on highly oriented pyrolytic graphite (HOPG) were taken by a JEOL JSEM-7400F probe station with an acceleration voltage of 10 kV under a vacuum condition of less than 10^{-4} Pa. Cast films for SEM and AFM measurements were prepared by dropping a portion of $CHCl_3$ solution of salt **2** (0.028 mM) on the HOPG surface with a rotation speed of 2000 rpm, which was fixed by conductive carbon tape at a sample stage. TG-DTA analyses of salts **1** and **2** were carried out by a Rigaku Thermo plus TG8120 thermal analysis station using an Al_2O_3 reference in the temperature range from 293 to 773 K with a heating rate of 5 $K min^{-1}$ under the nitrogen. 1H NMR spectra of salt **2** in $CDCl_3$ were measured by a Dionex DX-500 NMR spectrometer using an internal reference of TMS.

Preparation of Salt 2. Single crystals of salt **1** were prepared according to the literature.⁵ The salt **1** was identified by single-crystal X-ray structural analysis ($P1$, $a = 30.5577$, $b = 33.0363$, $c = 47.3963$ Å, $\alpha = 90.0540$, $\beta = 89.6920$, $\gamma = 96.8940^\circ$, $V = 47500.6$ Å³), XRD, and TG-DTA measurements. All reactions were carried out under a nitrogen atmosphere. Dimethyldioctadecylammonium chloride (DODA)(Cl) was purchased from Wako Chemicals Co., Ltd., and was used without further purification. Salt **2** was prepared by the cation exchange reaction of salt **1** in $CHCl_3/H_2O$ interface, and the blue solution of salt **1** in H_2O (1 g, 0.032 mmol in 100 mL) and 20 equiv of (DODA)(Cl) in $CHCl_3$ (0.38 g, 0.64 mmol) were mixed together and stirred for 1 h. After standing for a further 12 h, the organic layer was extracted and was dried over anhydrous $MgSO_4$. The resulting blue powder was precipitated by partial evaporation of $CHCl_3$, filtrated, and recrystallized from $CHCl_3-C_2H_5OH$ (0.68 g, 58% yield). 1H NMR ($CDCl_3$, δ): 0.88

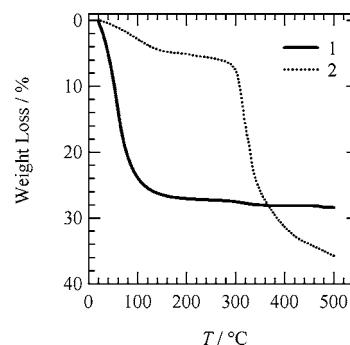


Figure 1. Thermogravimetry (TG) curves of salts **1** and **2**.

(6H), 1.26 (60H), 1.72 (4H), 3.43 (6H + 4H). IR (KBr): 3042, 2921, 2851, 1625, 1466, 974, 541, 507, 809, 718, 668, 637, 561 cm^{-1} .

Preparation of LB Films. The concentration of the spreading solution of salt **2** was fixed at 0.028 mM. Surface pressure (π)–area per molecule (A) isotherms were recorded at 291 K with a barrier speed of 100 $cm^2 min^{-1}$. HCl–KCl buffer solution adjusted to pH of 1.5 was employed for subphase of LB film preparations. The floating monolayers were left for 30 min after spreading and were transferred onto freshly cleaved mica surfaces at fixed surface pressures of 20 and 35 $mN m^{-1}$ by a single upstroke drawing for AFM measurements. Since the transfer ratio of LB films on quartz and CaF_2 substrates was less than 70% using a vertical-dipping method, a horizontal-lifting method was employed for the depositions of LB films on the hydrophobic substrates.

X-ray Diffraction and Scattering Measurements. Forty-layer LB films for the XRD measurements were deposited by the horizontal-lifting method on a hydrophobic glass. X-ray reflection diffraction (XRD) was measured using a Rigaku RINT-2000 diffractometer with $Cu K\alpha$ ($\lambda = 1.5418$ Å) radiation from a graphite monochromator in a 2θ scanning range from 1.00 to 60.0° with an interval of 0.02° and a scan speed of 2.00° min^{-1} . X-ray small-angle scattering was measured by a Rigaku Nanoviewer IP diffractometer with $Cu K\alpha$ ($\lambda = 1.5418$ Å) radiation from a graphite monochromator (40 kV \times 30 mA). A 0.025 wt % solution of salt **2** in THF was measured in a transmittance optical configuration. The scattering profile was analyzed by the Rigaku GXRR software package. An average diameter and a normalized variance were obtained by a least-squared method in a scanning range from 0.186° to 3.000° using a core–shell model with a structural factor of unity.

Optical Spectra. The 40-layer LB films were transferred by the horizontal-lifting method onto quartz and CaF_2 substrates (20 \times 13 mm^2) for the UV–vis–NIR and IR spectra, respectively. In the case of the UV–vis–NIR measurements, spectra taken with polarized lights parallel and perpendicular to the dipping direction with the incident angle at 0° were defined as 90p and 90s, respectively, and those with p- and s-polarized light with an incident angle at 45° as 45p and 45s, respectively. In the case of the IR measurements, transmission (T) and reflection–absorption (RA) spectra were measured on CaF_2 and evaporated gold substrates, respectively. The spectra consisted of 2000 scans with a resolution of 4 cm^{-1} using an MCT detector. The incident angle was fixed at 80° for the RA measurements.

Results and Discussion

Preparation and Characterization of Salt 2. The precursor $\{Mo_{154}\}$ -ring in crystalline state can be formulated, according to previous work,⁵ as $Na_{14}[Mo_{154}O_{462}H_{14}](H_2O)_{70} \cdot 400H_2O$ (**1**), and the inner one $\{Mo_2\}$ dimer site of salt **1** is reproducibly released as described previously.^{5,17} Figure 1 shows the temperature-dependent thermogravimetry (TG) curves of salts **1** and **2**. A rapid weight loss in the crystalline salt **1** was observed around room temperature by increasing of the temperature up

to 100 °C. The magnitude of weight loss from 30 to 150 °C (26.5%) was consistent with the total weight of H₂O molecules within the salt **1** (26.0%). Such a rapid elimination of H₂O molecules from the crystal made the salt **1** unstable. However, at the temperatures above 200 °C, the {Mo₁₅₄}-ring structure appears to be stable, since further weight loss from **2** was not observed.

A maximum of 28 DODA cations can be introduced from the number of sodium ions and protons of salt **1**. Therefore, 20 equiv of (DODA)(Cl) employed for the cation exchange reaction of salt **1** took part in forming salt **2**, giving a stoichiometry of (DODA)₂₀[Mo₁₅₄O₄₆₂H₈(H₂O)₇₀] (**2**), in which it can be reasoned that ca. eight protons will be present to balance the remaining negative charge. No stretching vibrations due to C–O groups were detected in the IR spectrum of salt **2**, suggesting that the recrystallization solvent ethanol was eliminated from the salt **2**, but a broad O–H stretching vibrational mode (ν_{OH}) of H₂O was observed at around 3025 cm⁻¹ (see Figure 7), indicating the incorporation of H₂O molecules into the salt **2**.¹⁸ The amount of H₂O molecule and DODA cations were further evaluated by the TG analysis, and the weight loss of 4.8% from room temperature to 170 °C corresponded to the elimination of about 90 H₂O molecules. This means that despite having been dried, compound **2** appears to have absorbed some extra 20 or so water molecules than the 70 water molecules incorporated into the structure of **1** and **2**. This is not unexpected, since the large cavity would provide an ideal environment to maintain a small droplet of 20 water molecules that could remain stable even if the compound was dissolved in organic solvents. A large weight loss of about 31.4% was observed by further increasing the temperature up to 400 °C. This is consistent with the loss of the 20 DODA present in (DODA)₂₀[Mo₁₅₄O₄₆₂H₈(H₂O)₉₀] (31.7%), and electronic spectroscopy confirms the mixed-valence electronic structure in **2** from the existence of Mo^V and Mo^{VI} ions within the {Mo₁₅₄}-ring.⁴ Therefore, it can be reasoned that the stoichiometry of (DODA)₂₀[Mo^V₁₂₆Mo^{VI}₂₈O₄₆₂H₈(H₂O)₇₀]·20H₂O of **2** is most consistent with our analytical data.

Structure of Salt 2 in Solution. The salt **1** was found to be soluble in H₂O, CH₃OH, C₂H₅OH, acetone, and CH₃CN, while salt **2** was soluble in common organic solvents such as acetone, CH₃CN, toluene, CH₂Cl₂, and CHCl₃. The chemical stabilities of salts **1** in H₂O and **2** in CHCl₃ were evaluated by the time-dependence of electronic absorption bands at 9.35 and 13.4 × 10³ cm⁻¹ (see Supporting Information). Although the spectral shapes of salts **1** and **2** were the same, the absorbance of salt **1** was found to decrease to half of its initial magnitude after 10 days, indicating gradual decomposition of the {Mo₁₅₄}-ring of salt **1** in H₂O. On the other hand, no spectral change of salt **2** in CHCl₃ was observed within 2 weeks, suggesting the high chemical stability of {Mo₁₅₄}-ring encapsulated by DODA cations in CHCl₃.

The structure of {Mo₁₅₄}-ring/DODA salts in CDCl₃ was examined by ¹H NMR (Figure 2). The electrostatic interaction between the {Mo₁₅₄}-ring polyanion and DODA cations dominates the structure of the salt **2** in solution. Both the chemical shifts and line widths of two methyl protons (6H) and α -CH₂ protons (4H) connected to the quaternary nitrogen atom changed upon the formation of the salt.^{13a} Those two signals of (DODA)-(Cl) were observed at 3.45 and 3.40 ppm, separately, while those of salt **2** shifted to lower field at 3.77 and 3.43 ppm and showed spectral broadening. The electrostatic interaction between the negatively charged {Mo₁₅₄}-ring and positively charged nitrogen

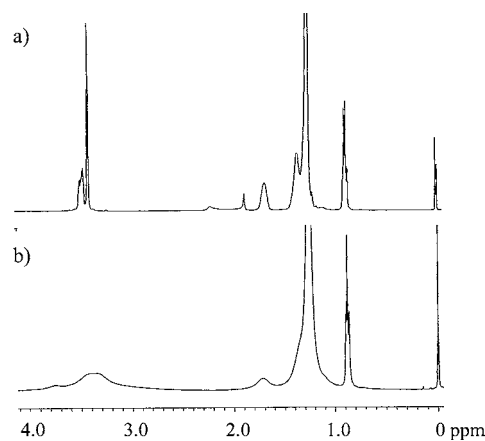


Figure 2. ¹H NMR spectra of (a) (DODA)(Cl) and (b) salt **2** in CDCl₃ at 298 K.

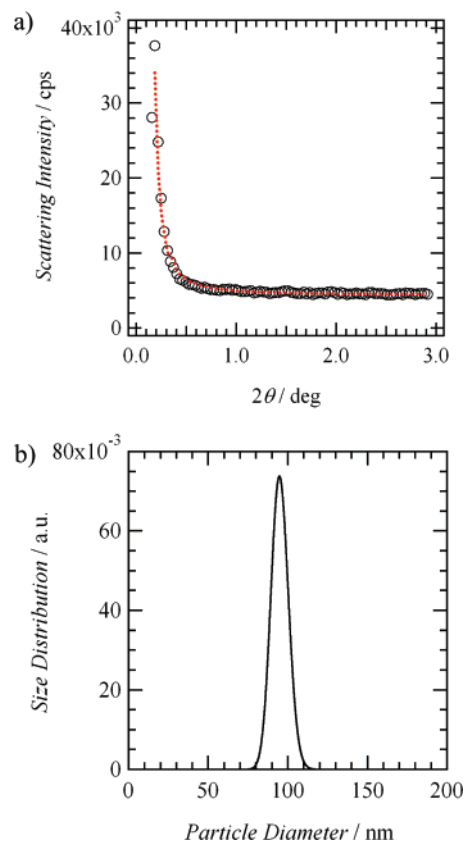


Figure 3. X-ray small-angle scattering of salt **2** in THF (6.5×10^{-6} M). (a) 2θ vs scattering intensity profile with a transmittance optical configuration. The red-line is a fitted using a core–shell model. (b) Size distribution of the diameter of vesicle-like molecular assemblies. The average diameter and normalized variance were 95 nm and 5.7%, respectively.

atom of DODA reduced the motional freedom of the head group of the DODA cation in solution, which caused the broadening and low field shift of the signals. Although the relatively large thermal motions of the two octadecyl chains were maintained in solution, the hydrophilic head groups of DODA cations were bounded to the surface of {Mo₁₅₄}-ring through the electrostatic interaction between the cations and polyanion in solution.

X-ray Small-Angle Scattering of Salt 2 in Solution. The molecular assembly structure of salt **2** in THF solution (6.5×10^{-6} M) was examined by X-ray small-angle scattering with a transmittance optical configuration. Figure 3a shows the scanning angle (2θ) vs scattering intensity (I) profile of salt **2** at the 2θ

(18) Jeffrey, G. A. *An Introduction to Hydrogen Bonding*; Oxford University Press: New York, 1997.

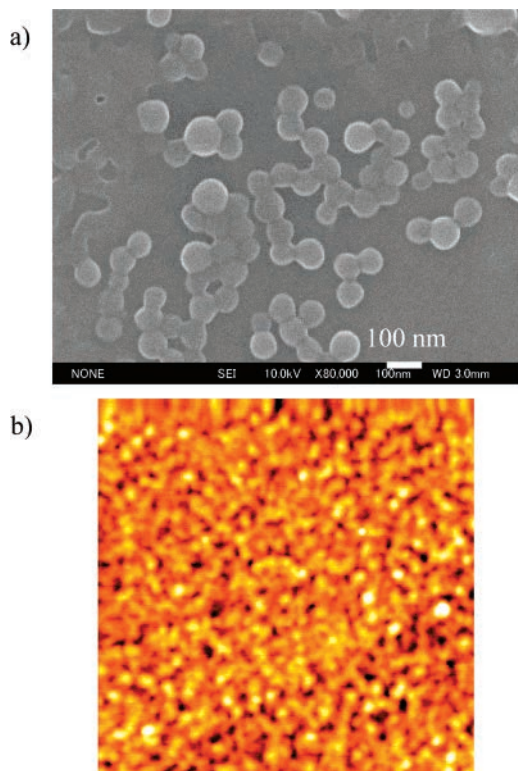


Figure 4. Images of the cast films of salt **2** on HOPG. (a) SEM image (scale bar = 100 nm) and (b) AFM image at $3 \times 3 \mu\text{m}^2$ scanning area.

range from 0.186° to 3.000° . The scattering intensity rapidly decreased at around $2\theta = 0.2^\circ$ by increasing the 2θ , where a damping coefficient in the 2θ - I profile corresponded to the density distribution of nanoscale molecular assemblies in homogeneous media.¹⁹ Since fine structure was not observed in the 2θ - I profile of salt **2**, the formation of relatively large size molecular assemblies can be postulated to occur in solution. Further, the negligible magnitude of intermolecular interaction between the molecular assembly structures can be assumed from a structural factor of unity due to the diluted measurement conditions. It is important to note in this context that the formation of vesicle-type molecular assemblies of salt **1**, $\{Mo_{72}Fe_{30}\}$ -ball, and $\{Mo_{144}\}$ -ring in H_2O have been confirmed by dynamic light scattering and SEM measurements already, where the gigantic POMs were arranged on the spherical vesicle surface through the lateral intercluster interactions.¹⁵ The formation of a vesicle-like molecular assembly of DODA- $\{Mo_{72}Fe_{30}\}$ hybrid system in $CHCl_3$ has been examined by Liu.²⁰ It is suggested that the electrostatic interaction between the $\{Mo_{72}Fe_{30}\}$ polyanions becomes a dominant factor in the formation of the vesicle-like "blackberry" assembly of gigantic clusters, while the hydrophobic DODA cations interact and stabilize the whole vesicle-like assembly.²⁰ A similar mechanism for aggregation of the $\{Mo_{176}\}$ -ring assembly was assumed in THF solution of salt **2**. Furthermore, the round-shaped molecular assemblies were confirmed on the substrate surfaces in the cast films of salt **2** (see below). Therefore, we assumed that the vesicle-like molecular assembly structures for salt **2** can also form in THF solution.

When the $\{Mo_{154}\}$ -ring is assembled on the spherical surface,¹⁵ the core and shell of vesicle are occupied by the solvent molecules and $\{Mo_{154}\}$ -rings, respectively. In this case, the densities of

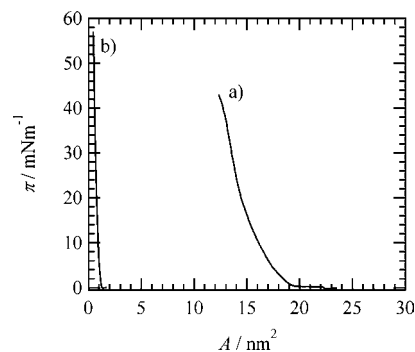


Figure 5. π - A isotherms of (a) salt **2** and (b) (DODA)(Cl) at the air-water interface ($T = 291$ K). The subphase was HCl-KCl buffer solution with a pH of 1.5.

core and of shell will be significantly different from each other. A similar molecular assembly is expected for the salt **2** in THF; therefore, the core-shell model was applied to analyze the 2θ vs I profile of salt **2**. Using this model, an average diameter of 95 nm with a normalized variance of 5.7% was obtained from the fitting (red-line) in Figure 3a, which was almost consistent with that of 90 nm of salt **1** in H_2O . Under the same measurement conditions, the gold nanoparticles prepared by the standard citric acid reduction method showed an average diameter of 13.4 nm and a normalized variance of 13.4%. The size distribution of vesicle-like molecular assembly of salt **2** was quite smaller than that of gold nanoparticles, indicating a significantly uniform spherical assembly structure of salt **2** in THF. Since the surface area of the sphere with the diameter of 95 nm was about 28 000 nm^2 , about 1400 ring molecule conjugates can be assembled on a spherical surface, assuming that the area per molecule of $(DODA)_{20}[Mo_{154}O_{462}H_8(H_2O)_{70}]$ is $\sim 19.8 \text{ nm}^2$ from the π - A isotherm at the air-water interface (see the section on floating monolayer below).

Molecular Assembly Structure of Salt **2** on Cast Films.

The high aggregation ability of salt **2** in solution is expected to encourage the formation of novel molecular assemblies on substrate surfaces. Therefore, surface morphologies of salt **2** in the cast films were evaluated by SEM and AFM measurements to investigate this idea.

Parts a and b of Figure 4 show the SEM and AFM images of the cast films on HOPG, respectively. The round-shaped domains were observed in both films. The average diameter of the round-shaped molecular assembly in the SEM image was about 100 nm, and the size distribution of domains is very small. Since the dimension of each domain on the HOPG surface was similar to that of vesicle-like molecular assembly in THF (~ 95 nm), it appears that the molecular assemblies in solution were fixed on the HOPG surface during the film fabrication processes. As the high-vacuum conditions of the SEM measurements completely removes the solvent molecules from the vesicle-like molecular assembly, the spherical core shell structure observed in solution is completely destroyed. Similar round-shaped molecular assemblies have been observed in SEM images of the cast films of $\{Mo_{144}\}$ - and $\{Mo_{154}\}$ -ring, whose diameters were distributed from 200 to 800 nm.¹⁵ Therefore, introduction of cations with hydrophobic properties in the $\{Mo_{154}\}$ -ring compound acts to increase the magnitude of intermolecular interactions and resulted in homogeneous molecular assemblies in solution as well as on substrate surfaces. Therefore, the hydrophobic interaction between the DODA cations plays an important role to stabilize assembly structures both in solution and cast film. The AFM images also support the formation of round-shaped molecular assemblies on a HOPG substrate (Figure 4b), and the collapse of the vesicle-

(19) (a) Parratt, L. G. *Phys. Rev.* **1954**, *95*, 359. (b) Croce, P.; Nevot, L. *Rev. Phys. Appl.* **1976**, *11*, 113.

(20) Liu, T. J. *Cluster Sci.* **2003**, *14*, 215.

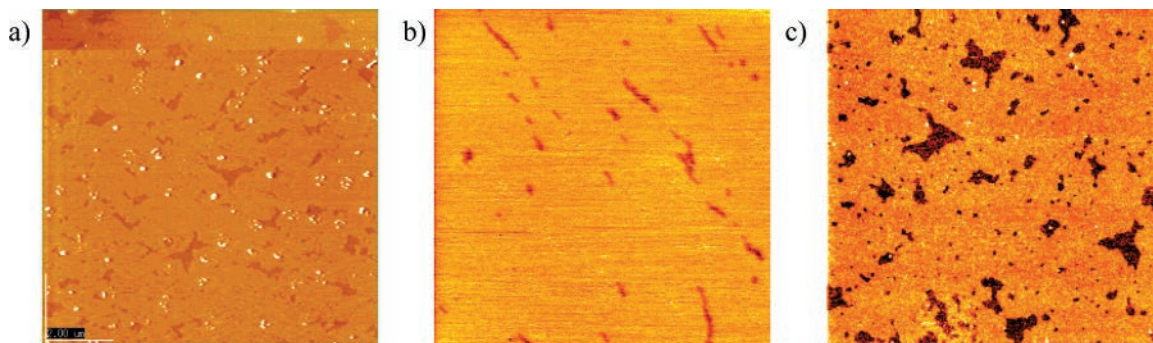


Figure 6. Surface images of LB monolayers of salt **2** transferred at the surface pressure of (a) 20 mN m^{-1} on mica ($5 \times 5 \mu\text{m}^2$), (b) 35 mN m^{-1} on mica ($3 \times 3 \mu\text{m}^2$), and 20 mN m^{-1} on Si substrate ($3 \times 3 \mu\text{m}^2$).

like molecular assembly yielded the round-shaped bilayer structure of salt **2** on substrate surfaces.

Molecular Assembly of Salt **2** at the Air–Water Interface.

Figure 5 shows the π – A isotherms of salt **2** and (DODA)(Cl) on the acidic buffer solution with a pH of 1.5 ($T = 291 \text{ K}$). Since the low reproducibility of the π – A isotherms of salt **2** on pure water suggested decomposition of $\{\text{Mo}_{154}\}$ -ring at the air–water interface, we employed the acidic buffer solution as the subphase. The acidic buffer solution stabilized the formations of the floating monolayer of salt **2** at the air–water interface. The π – A isotherm of (DODA)(Cl) indicated a sharp rise of the surface pressure at around $A = 1.2 \text{ nm}^2$ by lateral compression, and the areas per molecule at 20 and 35 mN m^{-1} were 0.97 and 0.90 nm^2 , respectively.²¹ A sharp π – A response around $A = 19 \text{ nm}^2$ was observed in salt **2**. Since the hydrophilic and hydrophobic moieties of salt **2** were $\{\text{Mo}_{154}\}$ -ring and DODA cations, respectively, the surface area in the π – A isotherm of salt **2** was dominated by the hydrophobic DODA cations. The surface area of salt **2** at 20 and 35 mN m^{-1} was 18.5 and 16.4 nm^2 , respectively. The area was about 20 times larger than those of (DODA)(Cl), which showed good correspondence with the proposed stoichiometry of the salt **2**, $(\text{DODA})_{20}[\text{Mo}_{154}\text{O}_{462}\text{H}_8(\text{H}_2\text{O})_{70}]$.

Langmuir–Blodgett Films of Salt **2** on Substrate Surfaces.

The floating monolayer of salt **2** was transferred onto the mica and Si substrates by a single withdrawal from the acidic subphase, the surface morphologies of which were observed by AFM measurements (Figure 6). Since the transfer ratios onto mica and Si substrate were almost unity in both cases, the floating monolayer of salt **2** was completely transferred onto the substrate surface. Although relatively homogeneous two-dimensional films of salt **2** were observed in the LB monolayer transferred at 20 mN m^{-1} on mica, the hollow surface areas were sometimes observed with an average depth of about 1.2 nm. Transfer of the monolayer of salt **2** at the air–water interface to the hydrophilic mica surface yielded a surface covered by the hydrophobic DODA cations. The heights of $\{\text{Mo}_{154}\}$ -ring and DODA cation were estimated at ~ 1.5 and $\sim 2.0 \text{ nm}$, respectively,²¹ and the depth of the hollow surface area was close to the height of the $\{\text{Mo}_{154}\}$ -ring. By increasing the surface pressure up to 35 mN m^{-1} , a highly homogeneous structure with almost complete absence of the hollow area was observed (Figure 6b). The depth of the hollow surface area decreased from 1.2 to 1.0 nm at 35 mN m^{-1} .

The floating monolayer of salt **2** could be transferred onto the hydrophilic Si substrate, whose surface was almost the same as that on mica substrate (Figure 6c). The two-dimensional molecular assembly of salt **2** at the air–water interface was transferred onto the substrate surface, which shows a key difference with

the case of cast film, in which spherical vesicle-like molecular assemblies in solution were fixed on the substrate surface as round-shaped domains. Therefore, it can be seen that the molecular assembly of the structures of salt **2** on the substrate surface can be controlled by the film-forming processes.

Electronic Structure and Molecular Orientation of Salt **2 in LB Films.** Since the transfer ratio of the deposition of the second layer was less than 0.7 by the vertical-dipping method, the horizontal-lifting method was employed for the fabrication of LB multilayers.²² The electronic structure and molecular orientation of the LB films were evaluated by the polarized optical spectra, AFM, and XRD measurements. A linear relationship between the absorbance of UV–vis–NIR spectra and deposition numbers indicated the good film-forming property of salt **2** (see Supporting Information). Figure 7a shows the electronic spectra of a 40-layer LB film of salt **2**. Two absorption bands at 9.35 and $13.4 \times 10^3 \text{ cm}^{-1}$ were the same as those of the salt **1**. These transitions were assigned to the charge-transfer (CT) transition between the pentavalent Mo^{V} and hexavalent Mo^{VI} ions within the mixed-valence $\{\text{Mo}_{154}\}$ -ring.^{14,23} The mixed-valence electronic structure of $\{\text{Mo}_{154}\}$ -ring was confirmed in the LB film of salt **2**.

The polarized absorption spectra of the LB film showed an isotropic absorbance for the 90s- and 90p-polarizations, while the intensity of the 45s-polarization was about 20% larger than that of the 45p-polarization. For the $\{\text{Mo}_{154}\}$ -ring, the sum of in-plan components of transition moments was larger than the sum of those perpendicular to the ring-plane. Therefore, the $\{\text{Mo}_{154}\}$ -ring plane within the LB film was relatively parallel to the substrate surface.²⁴

Figure 7b shows the transmittance IR spectrum in a KBr pellet and reflection–absorption (RA) IR spectra of LB film on evaporated gold substrate. The LB film transferred at 20 mN m^{-1} had the same spectral feature as that at 35 mN m^{-1} . The asymmetric and symmetric C–H stretching vibrational modes of CH_2 group (ν_{CH}) of DODA⁺ were observed at 2926 and 2854 cm^{-1} , respectively, while the C–H scissoring vibrational mode was observed at 1467 cm^{-1} .^{22,25} An intense vibrational band at

(22) (a) Petty, M. C. In *Langmuir–Blodgett Films: An Introduction*; Cambridge University Press: Cambridge, 1996. (b) Nakamura, T. In *Handbook of Organic Conductive Molecules and Polymers. Vol. 1 Charge-Transfer Salts, Fullerenes and Photoconductors*; Nalwa, H. S., Ed.; John Wiley & Sons: New York, 1997; p 728. (c) Ulman, A. *An Introduction to Ultrathin Organic Films*; Academic Press: San Diego, CA, 1991. (d) *Langmuir–Blodgett Films*; Roberts, G., Ed.; Plenum Press: New York, 1990.

(23) Müller, A.; Krickemeyer, E.; Bögge, H.; Schmidtman, M.; Beugholt, C.; Das, S. K.; Peters, F. *Chem. Eur. J.* **1999**, *5*, 1496 and references cited herein.

(24) (a) Matsumoto, M.; Nakamura, T.; Manada, E.; Kawabata, Y.; Ikegami, K.; Kuroda, S.; Sugi, M.; Saito, G. *Thin Solid Films* **1988**, *160*, 61. (b) Ikegami, K.; Kuroda, S.; Tabe, Y.; Saito, K.; Sugi, M.; Matsumoto, M.; Nakamura, T.; Kawabata, Y. *Jpn. J. Appl. Phys.* **1992**, *31*, 1206.

(25) Umemura, J.; Kamata, T.; Kawai, T.; Takenaka, T. *J. Phys. Chem.* **1990**, *94*, 62.

(21) (a) Eriksson, L. G. T.; Claesson, P. M.; Ohnishi, S.; Hato, M. *Thin Solid Films* **1997**, *300*, 240. (b) Abe, K.; Ohnishi, S. *Jpn. J. Appl. Phys.* **1997**, *36*, 6511. (c) Osman, M. A.; Ploetze, M.; Skrabal, P. *J. Phys. Chem. B* **2004**, *108*, 2580.

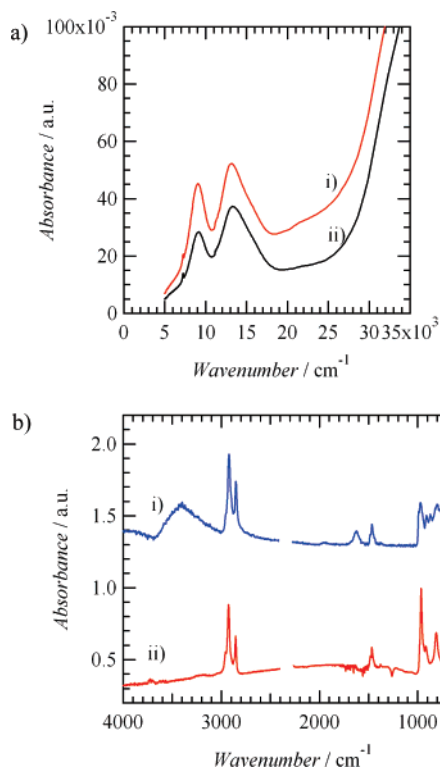


Figure 7. Optical spectra of salt **2**. (a) Polarized UV-vis-NIR spectra of 40-layer LB film at the optical configuration of (i) s-polarization and (ii) p-polarization with a 45° incidence. (b) Vibrational spectra of (i) solid state in KBr pellet (transmittance) and (ii) LB film transferred at 35 mN m^{-1} on evaporated gold substrate (reflection-absorption).

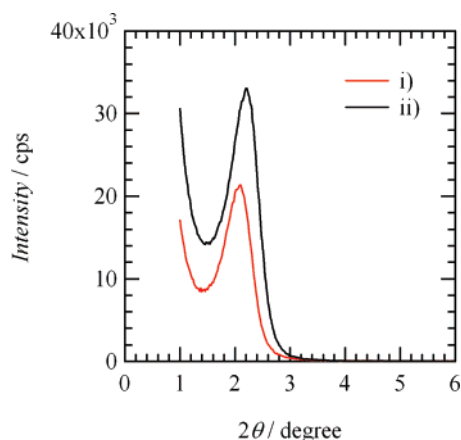


Figure 8. XRD profiles of LB films transferred at the surface pressure of (i) 20 mN m^{-1} and (ii) 35 mN m^{-1} .

965 cm^{-1} was assigned to the asymmetric stretching mode of Mo-O within the $\{Mo_{154}\}$ -ring. A distinct spectral difference between the LB film and solid was observed in the ν_{OH} mode of H_2O . Although the ν_{OH} was observed at 3412 cm^{-1} for the solid, that of the LB film almost disappeared. The H_2O molecules in the LB film were excluded from the $\{Mo_{154}\}$ -ring during the film depositions.

The periodicity along the film-forming direction of the LB film was evaluated from the XRD measurements (Figure 8). Since the LB films were fabricated by the horizontal-lifting method on the hydrophobic glass substrate, the X-type molecular orientation in the LB films was expected. The reflection peaks of LB films transferred at 20 and 35 mN m^{-1} were observed at $2\theta = 2.120^\circ$ and 2.220° , respectively, which correspond to the periodicities of 4.17 and 3.98 nm along the film-forming direction.

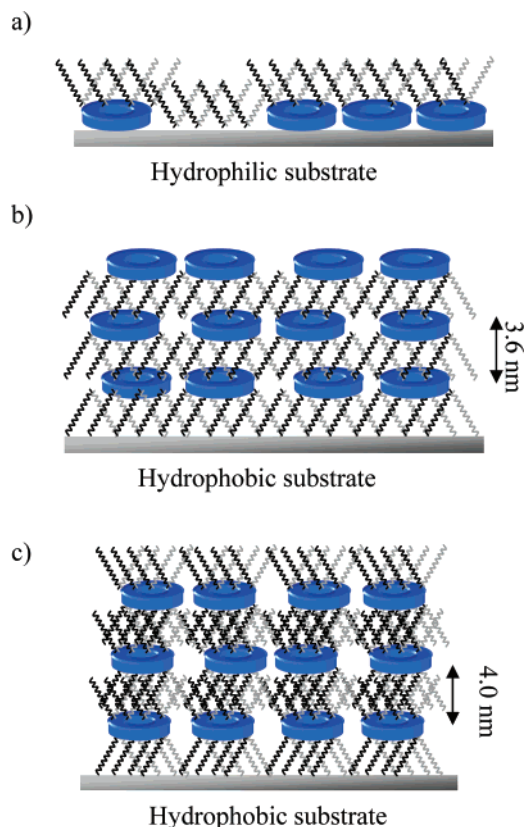


Figure 9. Schematic illustrations of the molecular orientation of salt **2**. (a) Molecular orientation on the hydrophilic substrate surface. The hollow surface area in AFM images corresponded to the surface area of DODA⁺ cations on the substrate surface. (b) X-type molecular orientation of LB film on the hydrophobic substrate surface. (c) Y-type interdigitated LB film with an interlayer spacing of $\sim 4 \text{ nm}$.

By increasing the surface pressure of film preparations, the periodicity along the film-forming direction slightly decreased, probably due to the dense packing structures of salt **2** within the LB film, which is consistent with the much more homogeneous surface morphology of LB monolayer transferred at 35 mN m^{-1} , as observed by AFM studies. In addition, an average height of about 4 nm from AFM measurements of LB monolayer prepared by the horizontal-lifting method (see Supporting Information) was consistent with the periodicity in the XRD measurements.

Molecular Assembly Structures of Salt 2. From the results of π -A isotherms, AFM images, polarized optical spectra, and periodicities in XRD, we can postulate the possible molecular orientations of salt **2** at the air-water interface and in the LB films. A calculated area on the $\{Mo_{154}\}$ -ring plane ($\sim 10.8 \text{ nm}^2$) is half of the sum of the area per molecule of 20 (DODA)(Cl) at the air-water interface of 20 mN m^{-1} ($0.97 \times 20 = 19.4 \text{ nm}^2$).

Within the transferred LB films, the $\{Mo_{154}\}$ -ring planes were arranged relatively parallel to the substrate surface from the polarized UV-vis-NIR spectra, while the alkyl chains of DODA were relatively perpendicular to the substrate surface (see Supporting Information). The thickness of $\{Mo_{154}\}$ -ring plane was about 1.5 nm , while the height of DODA cation on mica has been reported to be 2.0 – 2.1 nm .²¹ Therefore, the sum of heights of DODA cation and $\{Mo_{154}\}$ -ring was about 3.5 nm , assuming DODA cations lie on the $\{Mo_{154}\}$ -ring plane. In the transferred LB monolayer on mica, the hollow area observed by AFM with the depth of $\sim 1.2 \text{ nm}$ was close to the height of the $\{Mo_{154}\}$ -ring. Since the surface area of 20 DODA cations at the air-water interface was larger than that of the $\{Mo_{154}\}$ -ring, the

hollow surface area should be the domains of DODA cations laying on the $\{\text{Mo}_{154}\}$ -ring (Figure 9a). From the periodicity of ~ 4 nm along the film-forming direction (XRD measurement), the possible molecular arrangements in the LB films should be X-type (Figure 9b) or interdigitated Y-type (Figure 9c). Molecular rearrangements of DODA cations are necessary to form Y-type LB films, where each 10 DODA cations occupy the top and bottom surface area of the $\{\text{Mo}_{154}\}$ -ring plane. Since the area per molecule for 10 DODA cations was just fitted to the area of the $\{\text{Mo}_{154}\}$ -ring plane, the flip-flop motion of DODA cations should be one of the possible models. The interlayer spacing (3.6 nm) for X-type LB film (Figure 9b) was almost consistent with the periodicity of ~ 4 nm in the XRD measurement. In the Y-type LB film, two long alkyl chains of DODA cation should be interdigitated to each other, forming dense two-dimensional packing of DODA cations in order to form a layered structure with the periodicity of ~ 4 nm.

Summary

The mixed-valence gigantic polyoxometalate (POM) cluster of $\text{Na}_{14}[\text{Mo}_{154}\text{O}_{462}\text{H}_{14}(\text{H}_2\text{O})_{70}]\cdot 400\text{H}_2\text{O}$ (**1**) undergoes a cation metathesis reaction with surfactant cations of dimethyldioctadecylammonium (DODA), resulting in the formation of a mixed-valence solid of $(\text{DODA})_{20}[\text{Mo}_{154}\text{O}_{462}\text{H}_8(\text{H}_2\text{O})_{70}]$ (**2**). The high solubility of hydrophobic salt **2** to common organic solvents was confirmed, and the chemical stability of salt **2** in CHCl_3 was higher than that of salt **1** in H_2O . Effective electrostatic interactions between the $\{\text{Mo}_{154}\}$ -ring polyanion and DODA cations in CDCl_3 were observed in low field shift and broadening of methyl- and α -methylene protons connected to the positively charged nitrogen atom of DODA cation. Vesicle-like molecular assemblies of salt **2** with a small size distribution were observed in a diluted THF solution from the X-ray small-angle scattering. The diameter of vesicle-like molecular assembly was 95 nm with a normalized variance of 5.7%. The high aggregation ability of salt **2** in solution can be applied to the fabrication of molecular-assembly nano-

structures on substrate surfaces. The salt **2** in the cast film on HOPG formed round-shaped domains with an average diameter of ~ 100 nm, which were reflected by the vesicle-like molecular assemblies in solution. A stable floating monolayer of salt **2** at the air–water interface was transferred onto the substrate using the Langmuir–Blodgett technique. The area per molecule of salt **2** at the air–water interface was dominated by 20 DODA surfactants. The LB monolayer was transferred with a transfer ratio of unity on mica substrates, which formed two-dimensional films. The LB films of salt **2** had a mixed-valence electronic structure between the hexavalent Mo^{VI} ion and pentavalent Mo^{V} ion of $\{\text{Mo}_{154}\}$ -ring. Within the LB film, the $\{\text{Mo}_{154}\}$ -ring plane was relatively parallel to the substrate surface from the polarized optical spectra. The layer spacing along the film-forming direction of the LB films transferred by the horizontal-lifting method was consistent with the formation of X-type or interdigitated Y-type LB films. Two-dimensional molecular assemblies of salt **2** at the air–water interface were transferred onto the substrate surfaces by the LB method, while the vesicle-like spherical molecular assemblies were fixed at the substrate surface in the cast method. The assembly structures of salt **2** depended on the fabrication technique, reflecting assembly structures in solution or at the air–water interface.

Acknowledgment. This work was partly supported by a Grant-in-Aid for Science Research from the Ministries of Education, Culture, Sports, Science and Technology of Japan. T.A. thanks the Inamori Foundation for financial support and L.C. thanks the EPSRC and WestCHEM for support.

Supporting Information Available: The XRD, time-dependent UV–vis–NIR spectra, surface morphologies of AFM, transmittance vibrational spectra, and molecular orientation of alkyl chains in DODA^+ cations in the LB multilayers. This information is available free of charge via the Internet at <http://pubs.acs.org>.

LA701364K